Porous Graphitized Carbon Monolith as an Electrode Material for Probing Direct Bioelectrochemistry and Selective Detection of Hydrogen Peroxide

ARTICLE *in* ANALYTICAL CHEMISTRY · MARCH 2012

Impact Factor: 5.64 · DOI: 10.1021/ac203061m · Source: PubMed

analytical chemistry

Article

pubs.acs.org/ac

Porous Graphitized Carbon Monolith as an Electrode Material for Probing Direct Bioelectrochemistry and Selective Detection of Hydrogen Peroxide

Xiaoyun He,[†] Lin Zhou,[‡] Ekaterina P. Nesterenko,[†] Pavel N. Nesterenko,[§] Brett Paull,[§] Jesse O. Omamogho,[‡] Jeremy D. Glennon,[‡] and John H. T. Luong*[,‡,∥]

[†]Irish Separation Science Cluster, Dublin City University, Glasnevin, Dublin 9, Ireland

[‡]Irish Separation Science Cluster, Department of Chemistry and Analytical, Biological Chemistry Research Facility, University College Cork, Cork, Ireland

[§]Australian Centre for Research on Separation Science, University of Tasmania, Hobart, Australia

[∥]Biotechnology Research Institute, National Research Council, Montreal, Quebec, Canada

ABSTRACT: For the first time, graphitized carbon particles with a high surface area have been prepared and evaluated as a new material for probing direct electrochemistry of hemoglobin (Hb). Scanning electron microscopy (SEM) and transmission electron microscopy (TEM) imaging revealed that the carbon monolithic skeleton was constructed by a series of mesopores with irregular shapes and an average pore diameter of ~5.6 nm. With a surface area of 239.6 m^2/g, carbon particles exhibited three major Raman peaks as commonly observed for carbon nanotubes and other carbon materials, i.e., the sp^3 and sp^2 carbon phases coexisted in the sample. A glassy carbon electrode modified with carbon monoliths and didodecyldimethylammonium bromide exhibited direct electron transfer between Hb molecules and the underlying electrode with a transfer rate constant of 6.87 s^{-1}. The enzyme electrode displayed a pair of quasi-reversible reduction−oxidation peaks at −0.128 and −0.180 V, reflecting the well-known feature of the heme [Fe^{3+}/Fe^{2+}] redox couple: a surface-controlled electrochemical process with one electron transfer. This reagentless biosensing approach was capable of detecting H_2O_2, a simple molecule but plays an important role in analytical and biological chemistry, as low as 0.1 μM with linearity of 0.1−60 μM and a response time of <0.8 s, comparing favorably with other carbon based electrodes (5 s).

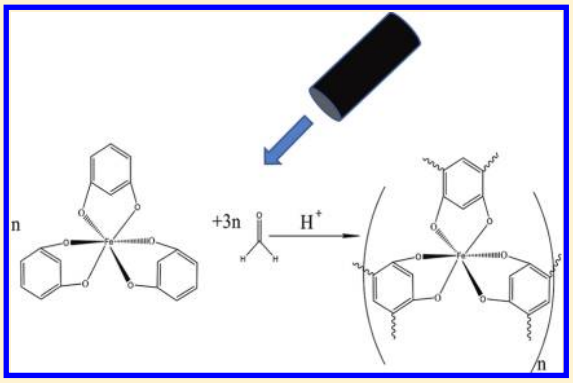

Direct electron transfer (ET) is of great interest toward the development of reagentless biosensing applications provided proteins/enzymes have redox-active centers accessible to the outer surface of the biomolecule for communication with the electrode. In principle, the ET can be achieved by controlling the biomolecule orientation to minimize the distance between its redox-active site and the electrode surface. However, the ET is difficult to attain because the prosthetic groups of the biomolecules are embedded deeply in the biomolecules. Nanomaterials with comparable sizes of enzymes/proteins hold great promise for controlling the biomolecular recognition for the achievement of direct electron transfer. Besides graphene and carbon nanotubes, porous carbon materials have attracted considerable interest in electrode modification owing to their high surface area, good electronic conductivity, chemical inertness, large potential window, and high electrocatalytic activity for many important redox reactions.[1−3] For instance, electrode materials such as carbon black,[4] carbon nanofibers,[5] and carbon nanochips[6] have been used for achieving the ET of hemoglobin. In addition, didodecyldimethylammonium bromide, a cationic surfactant, forms films resembling those of lipid membranes in living cells by simple casting onto electrodes, due to its controllable permeability and kinetic control of electrochemical reaction. The electron-transfer rate of myoglobin (Fe^{3+}/Fe^{2+}) at pyrolytic graphite electrodes is 1000-fold faster than that in solutions at $InSnO_2$ electrodes. Monolithic carbon is another class of carbon materials which can be prepared in any wet laboratory by pyrolyzing a copolymer of a resorcinol/iron(III) complex in the presence of silica particles.[7] Mesopores are formed in situ by the pyrolysis of the phenolic resin/iron complex. Macropores owing to the presence of silica beads in this bimodal structure can be eliminated and turned into flow-through pores by dissolving this material in hydrofluoric acid.

Hemoglobin (Hb), a four electroactive iron heme protein, plays also a major role in hemoglobinopathy and in anemia. Hb has been employed for the construction of reagentless biosensors for hydrogen peroxide, nitrile, nitric oxide, and

Received: November 17, 2011
Accepted: January 14, 2012
Published: January 25, 2012

   dx.doi.org/10.1021/ac203061m | *Anal. Chem.* 2012, 84, 2351−2357

trichloroacetic acid. Studies of electron transfer of Hb using different electrode materials are the most reported in the literature. However, the ET between Hb and the electrode is challenging due to its electroactive centers embedded deeply in the protein structure.[6,8] Therefore, it is very difficult to shuttle electron between the electrode surface with the active site of the enzyme without the use of an artificial mediator. The adsorption of protein molecules onto the bare electrode surface often leads to protein denaturation,[9,10] i.e., decreasing the direct electron-transfer rate.[11] Therefore, intensive efforts have been made to facilitate direct electrochemistry of this heme protein, using electrodes modified with functional inorganic nanomaterials, polymer films, and surfactants.

This paper describes direct electrochemistry of Hb on a glassy carbon electrode modified with graphitized porous carbon particles and bioelectrocatalytic activity for hydrogen peroxide, a byproduct of several important biochemical reactions and a signaling molecule in regulating diverse biological processes. Although carbon monoliths have been used in chromatography,[7] this work is the first attempt to reveal their applicability in electrochemistry to attain direct electrochemistry of Hb and subsequent selective detection of hydrogen peroxide. The structure, porosity, and surface area of carbon monolith fragments are characterized by scanning electron microscopy (SEM), transmission electron microscopy (TEM), BET nitrogen adsorption/desorption, and Raman spectroscopy.

EXPERIMENTAL SECTION

Materials. Hemoglobin (from bovine blood, H2625), didodecyldimethylammonium bromide (DDAB), resorcinol (99%), formaldehyde (37 wt % aqueous solution), HF acid (38−40%), sodium phosphate monobasic (NaH_2PO_4), and sodium phosphate dibasic (Na_2HPO_4) were obtained from Sigma-Aldrich (Dublin, Ireland). 1-Butanol and ferric chloride (99%) were obtained from Riedel-De Haen, Seelze (Hannover, Germany). Nucleosil 5 μm silica beads (surface area of 359 m^2/g and pore size of 550 Å) were obtained from Macherey−Nagel (Duren, Germany). A 0.1 M phosphate buffer solution (PBS), pH 7.0, was employed as the supporting electrolyte. Deionized water (18.2 MΩ·cm) was obtained from a Milli-Q (Millipore, Ireland) water purification system. All reagents were of analytical grade with highest purity.

Instrumentation. A GFL water bath, model 1013, from Laborgerateborse GmbH (Burladingen, Germany) was used to prepare the precursor carbon rod. An EHRET thermovacuum oven from Ehret Labor and Pharmatechnik GmbH, KG, Emmendingen, Germany was used to complete the polymerization of the precursor carbon rod. For the pyrolysis of the rod, a desktop alumina tube furnace, model GSL1300X, from MTI (Richmond, VA, U.S.A.) was used. The surface morphology of the carbon monoliths was examined using a Hitachi SEM/energy-dispersive X-ray spectroscope (SEM/EDX), model S-3000N VP, Oxford, U.K. High-resolution SEM images of the monolith surface morphology were achieved using a field emission Hitachi S-5500 SEM (Hitachi High Technologies America, U.S.A.). A surface area analyzer, model TriStar II 3020 (Micromeritics Gemini, Georgia, U.S.A.), was used to measure the specific surface area and the pore volume using the nitrogen adsorption/desorption technique. Typically, a 20 mg piece of carbon monolith rod was dried and loaded into the apparatus for the measurement. The Raman spectrum was performed on a LabRam800HR (Horiba Jobin Yvon, Northampton, U.K.). The Ar ion laser user as the excitation source is the Innova 70-C-2 made by Coherent. The laser power was 6 mW. High-resolution imaging for carbon monoliths was also performed by using the JEM-2000FX II (Jeol, U.K. Ltd.) transmission electron microscope (TEM) operated at 200 kV. The instrument is equipped with a MegaView III camera for obtaining digital images controlled by the AnalySIS software (Soft Imaging Systems GmbH). About 1 mg of pulverized carbon monolith was dispersed in 3.5 mL of methanol and sonicated for 10 min. A small drop of the carbon powder solution was added to a carbon film coated copper TEM grid which allowed the solvent to evaporate at atmospheric pressure and room temperature.

Fabrication of Carbon Monolith Rods. A modified procedure was used for the preparation of the carbon monolith (CM) rods.[12] A 1 g portion of silica particles (5 μm) was dispersed in 1.5 g of 1-butanol and sonicated for 1 h. An 0.18 g portion of ferric chloride followed by the addition of 0.367 g of resorcinol was then added into the silica suspension and dissolved by gentle shaking. After the addition of resorcinol, the resulting solution turned dark quickly to form a resorcinol/Fe (III) complex (Figure 1). A 0.3 g portion of an ice-cooled, 37%

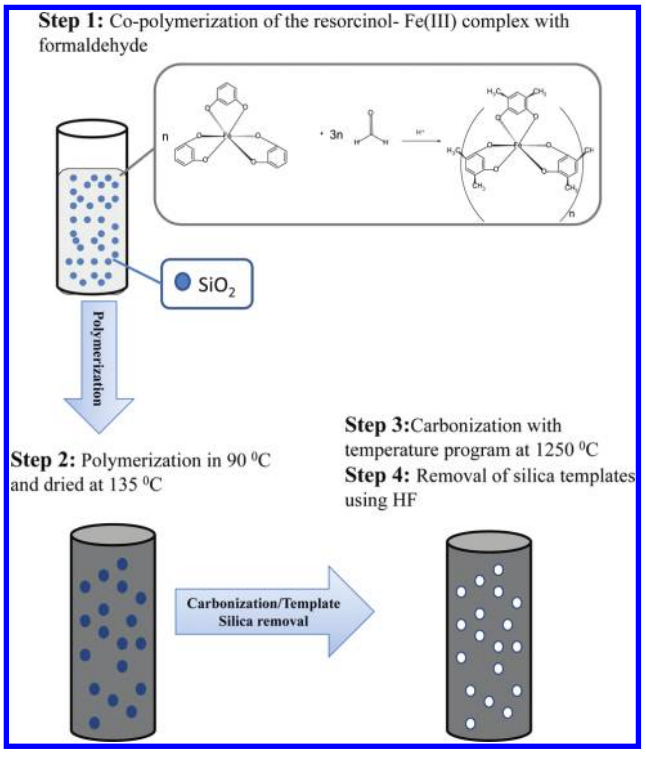

Figure 1. Scheme for the preparation and pyrolysis of the carbon monolith rod.

formaldehyde solution in water was introduced into the mixture in one step with further gentle agitation. The mixture was kept in an ice−water bath for 1 h with constant stirring. After removal from the ice−water bath, the mixture was slowly transferred into 7 mm i.d. glass tubes which were capped when filled. These tubes were then placed in a 90 °C hot water bath for 15 h. The mixture polymerized into a solid rod inside the glass tube. The resin rod was detached from the glass tube wall due to its shrinking caused by polymerization. Crack-free phenolic resin/silica rods were then removed from the glass tubes and kept in the fume hood for 72 h to slowly evaporate

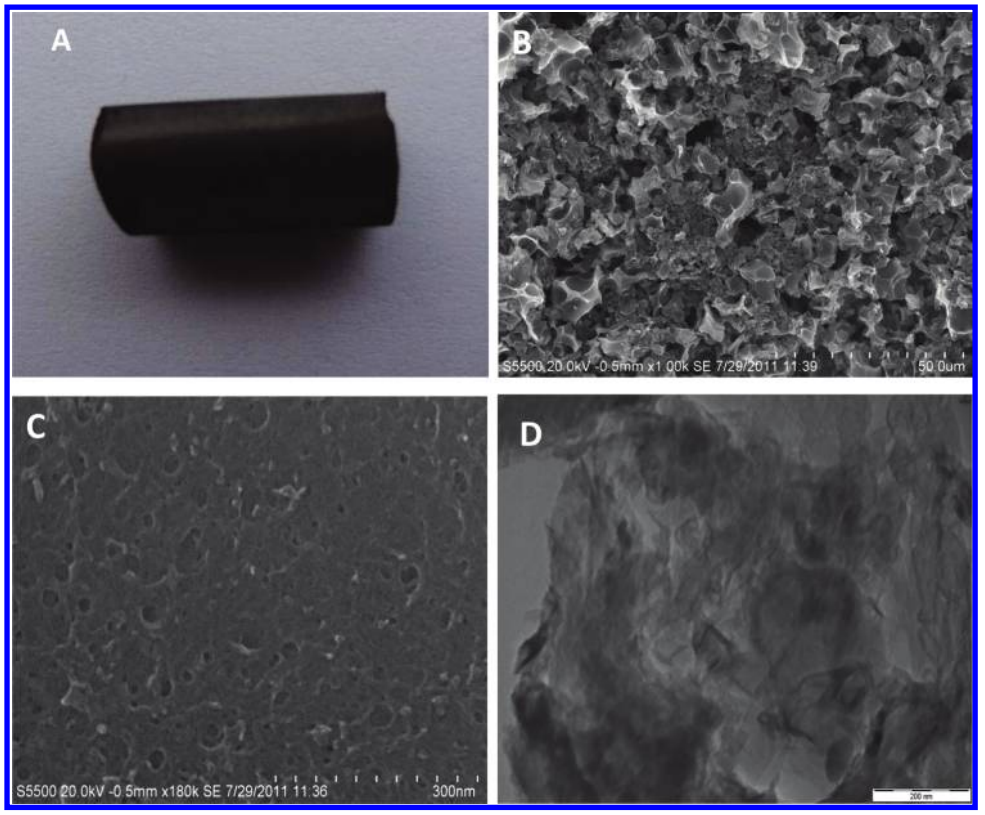

Figure 2. (A) Photo of a typical carbon monolith rod. (B) SEM images of carbon monolith fragments with low (×1K) magnification. (C) SEM images of carbon monolith fragments with high (×180K) magnification. (D) A representative TEM micrograph of carbon monolith.

the majority of the residual solvent. Finally, the rods were thoroughly dried in a vacuum oven at 80 °C overnight and further cured at 135 °C for 4 h to ensure complete polymerization.

A horizontal tube furnace purged with N_2 gas was employed to pyrolyze the rods. The temperature was first ramped from room temperature to 800 °C at 2.5 °C/min and then held at this temperature for 2 h to ensure complete carbonization. A second ramp took place from 800 to 1250 °C at 10 °C/min, and this temperature was kept for another 1 h. The furnace was allowed to cool naturally to room temperature. Silica particles and the iron catalyst were removed from the rods by etching in concentrated HF acid (38−40%) for 5 h and subsequently washed away with copious amounts of deionized water to attain neutral pH. The porous carbon rods obtained were then thoroughly dried under vacuum at 80 °C for 16 h.

Enzyme Electrode Preparation. A glassy carbon (GC) electrode (3 mm in diameter, BAS, West Layette, IN) was polished on a polishing cloth with 0.3 and 0.05 μm alumina powder, respectively, and rinsed with deionized water followed by sonicating in ethanol and deionized water. The electrode was dried with a purified nitrogen stream. Carbon monolithic fragments (CM) were prepared by crushed the carbon monolith rod by a mortar and pestle. An Hb solution (10 mg mL^{-1} in 0.1 M pH 7.0 PBS) and a CM−DDAB solution (10 mg mL^{-1} in 10 mM DDAB) were mixed by 1:1 ratio. DDAB has been proved to be a good surfactant for immobilizing hemoglobin on the glassy carbon electrode.[13] DDAB has been used to modify mesoporous carbon[14] and combined with room temperature ionic liquid for immobilization of hemoglobin.[15]

The suspension (5 μL) was cast onto the surface of the freshly polished GC electrode (Hb/CM−DDAB/GC). Water was evaporated slowly in air, resulting in a uniform film electrode. The Hb/DDAB/GC and Hb/GC electrodes were prepared by the same method. The dried electrodes were stored at 4 °C when not in use.

Amperometric Measurement. Amperometric (I/t) and cyclic voltammetry (CV) measurements were performed using a CHI 1040A electrochemical workstation (CH Instruments, Austin, TX) at room temperature. A three-electrode system consists of a glassy carbon working electrode, a Ag/AgCl (3 M NaCl) reference electrode (BAS, West Layette, IN), and a platinum wire counter electrode (Sigma-Aldrich, Dublin, Ireland). The convective transport during the amperometric determination was performed with magnetic stirring at 800 rpm. The buffer solution was purged with highly purified nitrogen for at least 30 min, and a nitrogen atmosphere environment was kept during the course of measurement.

RESULTS AND DISCUSSION

Characterization for Carbon Monolith. Combined polymerization and pyrolysis was capable of producing carbon monolith of up to 100 mm in length (length of the glass tube) without internal and surface fissures or crack. The monolith rod exhibited a smooth homogeneous surface as shown Figure 2A. As revealed by SEM imaging with low magnification (×1K) of the monolith rod in cross section, the synthesized carbon monolithic (CM) fragments possessed a well-defined three-dimensional (3D) structure. The CM skeleton was constructed by a series of mesopores with irregular shapes except for a few micropores on the walls (Figure 2B). On the basis of high-magnification SEM imaging (×180K), the pores were estimated to be ∼5.6 nm or mesopores (Figure 2C), in agreement with the BET results as discussed later. TEM imaging also confirmed

dx.doi.org/10.1021/ac203061m | Anal. Chem. 2012, 84, 2351−2357

Table 1. Energy-Dispersive X-ray Spectroscopy (EDX) of a Typical Carbon Monolith Rod

sample	C	O	F	Al	Si	Cl	Fe	Cu	total
1	84.71	9.60	5.29	0.02	0.27	0.02	0.03	0.06	100
2	90.97	8.20	0.64	0.00	0.03	0.01	0.04	0.10	100
3	65.86	4.74	29.32	0.01	0.02	0.00	0.00	0.05	100

the porous nature and irregular shapes of CM (Figure 2D). EDX analysis further attested negligible iron impurities from three different CM fragments (Table 1). This was an important finding since the presence of iron, even as a trace element, is involved in electron transfer occurring at the clay surface, affecting the response and reproducibility of Hb–clay modified electrodes.[16] Silica particles were completely removed from the carbon rod after HF acid etching.

The BET measurement confirmed that there was no sharp condensation/evaporation step or a pronounced hysteresis loop in the isotherm, which is often observed for materials with a narrow pore size distribution (Figure 3A). It was reasoned that

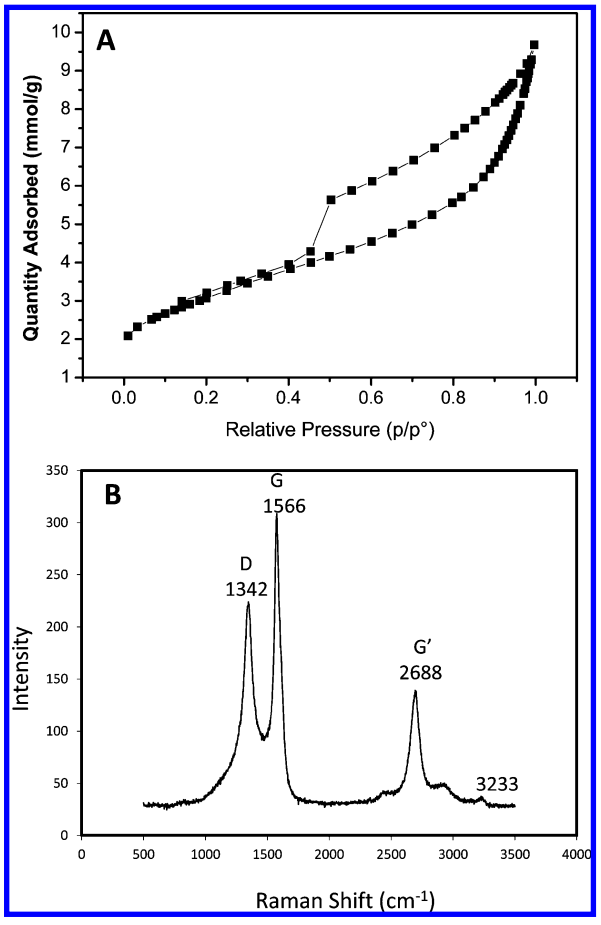

Figure 3. (A) Typical BET isotherm of carbon monolith fragments. (B) Raman signature of carbon monolith fragments.

the voids between graphite strips were not controllable; therefore, the pores between graphite strips could have any size and shape. The BET surface area of the carbon monolith rod was 239.6 m^2/g, significantly higher than the value reported by Liang et al. (162.9 m^2/g).[7] After crushing the carbon monolith rod, the BET surface area of the carbon monolithic fragments was 138.8 m^2/g. Apparently, the combination of mesopores and micropores with a high surface area makes carbon monolithic particles a potential material for biomolecule immobilization and biosensing applications.

The Raman signature of CM exhibited three major peaks as commonly observed for carbon nanotubes and other carbon materials, i.e., the sp^3 and sp^2 carbon phases coexist in the sample (Figure 3B). The D mode, the disorder band, is located at 1342 cm^{-1}, which is active in Raman as the result of the imperfection of the graphite. For single-walled carbon nanotubes, the presence of this peak can be attributed to defects in the tubes. For highly oriented pyrolytic graphite (HOPG), the D peak is very small or negligible. The G mode or (TM—tangential mode), common to all sp^2 carbon forms, observed at 1566 cm^{-1}, corresponds to the stretching mode of the C–C bond in graphitic materials. In amorphous carbon, this peak is broadened and shifted to 1600 cm^{-1}.[17] The peak located at 2688 cm^{-1}, or the G′ band, a second-order two-phonon process, was expected for all kinds of sp^2 carbon materials which normally appear in the range of 2500–2800 cm^{-1}. The coherence length (L_a), estimated using the Tuinstra–Koenig relationship or L_a (nm) = $(2.4 \times 10^{-10})\lambda^4_{laser}(I_D/I_G)^{-1}$, was 23.2 nm, which is slightly lower than the value of commercial graphite (31.7 nm).

Direct Electrochemistry. Bovine Hb is a hemoprotein with a molecular weight of 68 kDa, an isoelectric point (IP) of 7.1, and ellipsoidal diameters of 70 × 55 × 55 $Å^3$.[18] This heme protein can be adsorbed on clays with a maximum capacity when the pH of suspension (pH 7.0) corresponds to the IP of the protein.[19,20] Figure 4A shows the cyclic voltammograms (CV) of different electrodes in 0.1 M PBS, pH 7.0, at 100 mV s^{-1}. As expected, the CV of Hb/GCE was featureless (Figure 4A, curve a) compared to a pair of quasi-reversible reduction–oxidation peaks observed at Hb/DDAB/GCE. The peaks at −0.128 and −0.180 V were stable and well-defined (Figure 4A, curve b). The formal potential ($E^{\circ\prime}$) of the Hb/DDAB/GC electrode was −0.154 V versus Ag/AgCl, reflecting the well-known potential characteristic of heme–Fe^{3+} + e^- → heme–Fe^{2+} redox couples.[21] Thus, besides its role for the immobilization of Hb, the surfactant also facilitated the direct electron transfer between the protein and the electrode. However, for the Hb/CM–DDAB/GC electrode, the redox peak current was significantly enhanced (Figure 4A, curve c). Such a result could be attributed to the high surface area of CM and the entrapment of Hb in the nanocomposite film exhibited high electrochemical activity.

Figure 4B shows the cyclic voltammograms of Hb/CM–DDAB/GCE with different scan rates in pH 7.0 PBS. A pair of roughly symmetric redox peaks appeared with almost equal heights of the redox peak currents in the scan rate from 20 to 500 mV s^{-1}. The results indicated that all the electroactive Hb Fe(III) in the film was reduced to Hb Fe(II) on the forward scan and reoxidized to Hb Fe(III) on the reverse scan. A good linear relationship was observed (Figure 4B, inset) between the redox peak current and the scan rate with the results as I_{pa} (μA) = 0.0055υ (mV s^{-1}) + 0.1422 (r = 0.997) and I_{pc} (μA) = −0.0058υ (mV s^{-1}) − 0.373 (r = 0.997). Such behavior revealed that the electron transfer between Hb and GCE was a

dx.doi.org/10.1021/ac203061m | Anal. Chem. 2012, 84, 2351–2357

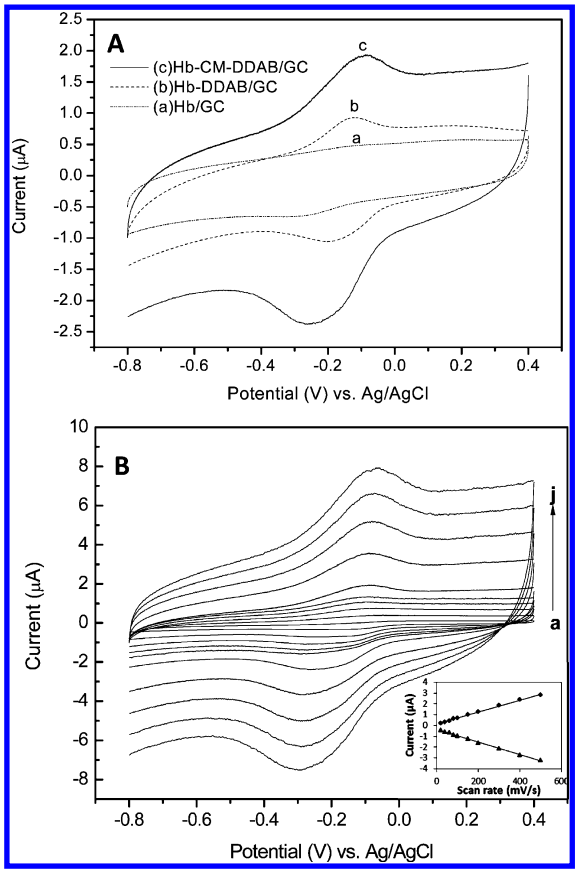

Figure 4. (A) Cyclic voltammograms (CV) of (a) Hb/GC electrode, (b) Hb/DDAB/GC electrode, (c) Hb/CM−DDAB/GC electrode in 0.1 M PBS pH 7.0 at the scan rate of 100 mV s^{-1}. (B) Cyclic voltammograms of the Hb/CM−DDAB/GC electrode in 0.1 M PBS (pH 7.0) at different scan rates. Scan rate (from a to j): 20, 40, 60, 80, 100, 150, 200, 300, 400, and 500 mV s^{-1}. Inset: plots of peak current vs scan rates.

surface-controlled electrochemical process and the immobilized Hb on CM−DDAB film was not denatured as commonly observed with other electrode materials.[22]

The formal potential ($E^{0\prime}$), calculated from the midpoint of the reduction and oxidation peak potentials, was −184 mV (vs Ag/AgCl), and the peak-to-peak potential difference (ΔE_p) was 116 mV. Such information thus confirmed that Hb immobilized on the CM−DDAB/GC electrode displayed a quasi-reversible electrochemical reaction. On the basis of the integration of the cyclic voltammetric reduction peaks and Faraday's laws, the surface concentration (Γ, mol cm^{-2}) of the electroactive substance was estimated as[23]

$$Q = nFA\Gamma \tag{1}$$

$$I_p = \frac{n^2F^2\upsilon A\Gamma}{4RT} = \frac{nFQ\upsilon}{4RT} \tag{2}$$

where Q is the total amount of charge passed through the electrode for the reduction reaction, n is the number of electrons transferred, F is the Faraday's constant, υ is the scan rate, and A is the geometric area of GCE (0.0707 cm^2, 3 mm in diameter). Considering the amount of Hb used (5 μL, 5 mg/mL, MW 68 000) for the construction of the Hb electrode, the expected amount of the hemoglobin immobilized on the electrode was 5.2 × 10^{-9} mol cm^{-2}. The apparent surface concentration (Γ) of the electroactive Hb was estimated by calculating the total charge involved in the anodic or cathodic current peak at 100 mV s^{-1}. The apparent surface concentration of Hb/CM−DDAB/GC was 3.4 × 10^{-9} mol cm^{-2} or 70% of the expected amount of Hb on the electrode surface (5.2 × 10^{-9} mol cm^{-2}), i.e., most of the Hb molecules retained their bioactivity in the film. Laviron's method[24] was used to estimate the apparent heterogeneous electron-transfer rate constant (k_s).

$$\log k_s = \alpha \log(1-\alpha) + (1-\alpha)\log\alpha - \log\frac{RT}{nF\upsilon} - \alpha(1-\alpha)\log\frac{nF\Delta E_p}{2.3RT} \tag{3}$$

The values of α and k_s were estimated to be 0.5 and 6.874 s^{-1}, respectively. The electron-transfer rate constant was significantly higher than the value reported for Hb carbon material sensors: 1.02 s^{-1} for a carbon black modified GC electrode[4] and 0.062 s^{-1} for a carbon nanotube modified GC electrode.[25] Such a result illustrated that carbon monolith fragments effectively promoted the electron transfer between Hb and the modified electrode surface.

Electrocatalysis. Hb/CM−DDAB/GCE was then evaluated for the detection of hydrogen peroxide, an analyte that plays an important role in the pharmaceutical and chemical industry as a bleaching, oxidizing, and sterilizing agent. In living organisms, H_2O_2 serves as a signaling molecule to regulate diverse biological processes such as immune cell activation, vascular remodeling, apoptosis, stomatal closure, and root growth. This simple molecule is also a byproduct of several biochemical reactions catalyzed by glucose oxidase, alcohol oxidase, lactate oxidase, urate oxidase, cholesterol oxidase, glutamate oxidase, amino acid oxidases, etc. Current analytical procedures for H_2O_2 such as fluorescence, chemiluminescence, and absorbance are complex, time-consuming, and vulnerable to interference. In contrast, electrochemistry is simple, sensitive, and cost-effective. Therefore, the detection of this analyte is an important task in various industries including textiles, food, and pharmaceutics. With Hb, the detection is based on the well-known detection scheme as follows:[26,27]

$$Hb(Fe^{3+}) + H_2O_2 \rightarrow \text{intermediate I } (Fe^{4+}{=}O) + H_2O_2 \tag{4}$$

$$\text{intermediate I } (Fe^{4+}{=}O) + e^- + H^+ \rightarrow \text{intermediate II} \tag{5}$$

$$\text{intermediate II} + e^- + H^+ \rightarrow Hb(Fe^{3+}) + H_2O \tag{6}$$

Figure 5A shows cyclic voltammograms of the modified electrode in the absence and presence of H_2O_2. The addition of H_2O_2 to the catalytic cell resulted in the disappearance of the oxidation peak, whereas there was an increase of the reduction peak, depending on the concentration of H_2O_2 in solution. Such a result confirmed that Hb was retained on the CM modified electrode with pseudoperoxidase activity. At the Hb/CM modified GC electrode, reduction response commenced at −0.05 V followed by an obvious catalytic reduction peak at −0.25 V. The reduction of overvoltage and increasing the peak current of hydrogen peroxide reduction confirmed that Hb exhibited high catalytic ability for H_2O_2 reduction.

At −0.3 V applied potential, the enzyme electrode exhibited a detection limit of 0.1 μM (3 S/N) with linearity of 0.1−60 μM for H_2O_2 (Figure 5B). After the substrate addition, the

dx.doi.org/10.1021/ac203061m | Anal. Chem. 2012, 84, 2351−2357

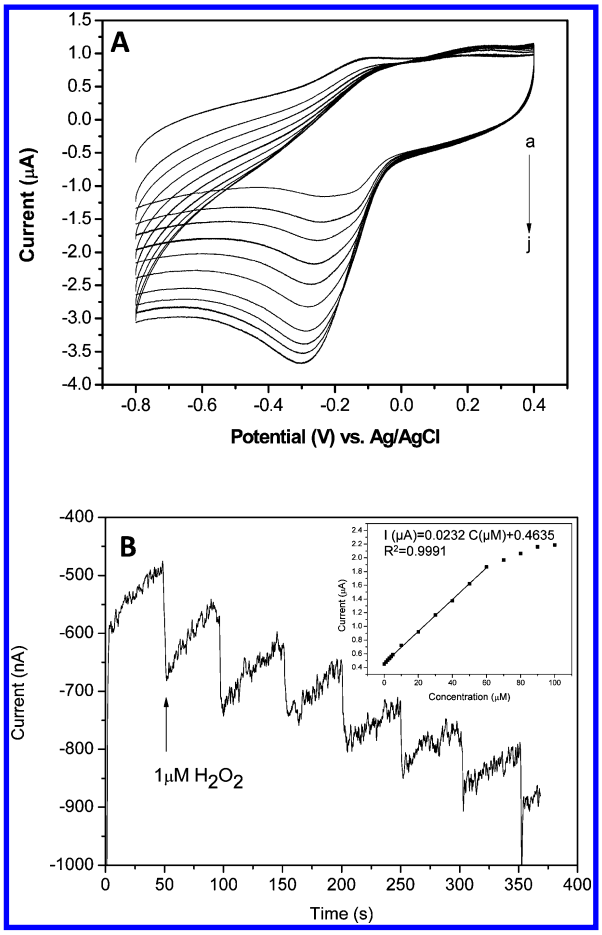

Figure 5. (A) Cyclic voltammograms (CV) of the Hb/CM−DDAB/GC electrode in 0.1 M PBS (pH 7.0) with (a−j) 0, 10, 20, 30, 40, 50, 60, 70, 80, 90, and 100 μM H_2O_2, scan rate 100 mV s^{-1}. (B) Amperometric detection (I/t) of 1 μM H_2O_2 in 0.1 M PBS, pH 7.0, by the Hb/CM−DDAB/GC electrode at −0.3 V vs Ag/AgCl (3 M KCl). Inset: the calibration curve of different concentrations of H_2O_2.

biosensor displayed a response time of 0.8 s, and the current was measured on the plateau corresponding to the steady state. It should be noted that the baseline shown in Figure 5 did not return to a constant level due to the presence of dissolved oxygen when hydrogen peroxide was added to the electrolytic cell. Therefore, the calibration curve was established from a single measurement (performed in triplicate) by adding different amounts of hydrogen peroxide (up to 100 μM) to a fresh electrolyte after nitrogen purging to circumvent oxygen interference. It was confirmed that relevant physiological levels (0.1 mM) of three common interfering species, uric acid, ascorbic acid, and acetaminophen, resulted in no response, i.e., the biosensing scheme is applicable for detecting hydrogen peroxide of biological samples. The apparent Michaelis−Menten constant (K_m^{app}), a reflection of the enzyme−substrate kinetics, was calculated by the Lineweaver−Burk equation:[28]

$$1/I_{ss} = 1/I_{max} + K_m^{app}/I_{max}C \quad (7)$$

where I_{ss} is the steady current after the substrate addition, C is the bulk concentration of the substrate, and I_{max} is the maximum current measured under the saturated substrate condition. The apparent Michaelis−Menten constant (K_m^{app}) was 18 μM, implying that this biosensor exhibited high affinity to H_2O_2 and outperformed the carbon nanotube modified GCE.[25]

To study the reproducibility of Hb/CM−DDAB/GCE, repetitive measurements were carried out for 5 μM H_2O_2. A relative standard deviation of 3% was obtained for 20 successive measurements. When stored at 4 °C, the Hb/CM−DDAB/GC electrode only decreased about 1% of its initial response after 2 days and still retained over 95% of its original activity after 1 week. A standard deviation of 7% was observed from five different Hb/CM−DDAB/GC electrodes.

CONCLUSION

Graphitized carbon monoliths with a high surface area have been used as a new material for immobilization of Hb and modification of the glassy carbon surface. We have shown for the first time that the introduction of CM enhanced the electron transfer between Hb molecules and the underlying electrode, due to the excellent electrical conductivity of CM and its biocompatibility. CM holds great promise for the use of Hb or other heme proteins such as horseradish peroxidase, catalase, cytochrome *c*, microperoxidas, and myoglobin. Like Hb, such metalloproteins contain iron-centered porphyrin as their prosthetic groups.

Table 2. Comparison of the Hb/CM−DDAB Electrode with the Literature Data for Peroxidase-like Activity

film	linear range (μM)	detection limit (μM)	response time (s)	K_m^{app} (μM)	ref
Hb/CM−DDAB	0.1−60	0.1	0.8	18	this work
Hb/CNT	210−900	9	na	675	25
Hb/graphene−chitosan	6.5−230	0.51	5	230	32
Hb/ZrO_2/DMSO	1.5−30.2	0.14	na	310	33
Hb/titanium sol−gel	0.5−54	0.12	na	na	34
Hb/carbon nanochip	0.5−30	0.05	5	21.55	6
Hb/nanocarbon	0.9−17	0.4	na		35
Hb/AuNFs	1.0−60	7.3	na	10.35	36

Of also particular interest is the excellent catalytic activity toward several important analytes such as hydrogen peroxide,[29] nitrite,[30] and nitric oxide.[31] The utilization of electrocatalytic activity of carbon monoliths effectively reduces the overpotential oxidation for H_2O_2, thus alleviating severe interferences from electroactive species. Carbon monoliths can be fabricated in different sizes and shapes and modified for in vivo measurement to provide appropriate spatial and temporal resolution within acceptable sensitivity and limits of detection. Easy and simple fabrication, low cost, and excellent electrochemical catalysis with higher selectivity are all obvious advantages for this newly proposed modified electrode. Therefore, carbon monolith should have a great potential for the development of new sensing schemes and devices to solve many analytical problems. As electron transfer is ubiquitous in chemical and biological systems, carbon monolith is expected to play an important role in understanding and controlling of this process, one of the broadest and most active research areas of science. Carbon monoliths might be considered as a new class

dx.doi.org/10.1021/ac203061m | *Anal. Chem.* 2012, 84, 2351−2357

of carbon electrode materials besides glassy carbon, carbon paste, carbon nanotubes, graphene, and boron-doped diamond (Table 2). However, unlike graphene or carbon nanotubes, the fabrication of carbon monoliths does not require any tedious and time-consuming postpurification step. Therefore, carbon monoliths with high surface area could be applicable in large-scale electrochemical systems such as fuel cells, electrosynthesis, and electrochemical remediation.

AUTHOR INFORMATION

Notes

The authors declare no competing financial interest.

ACKNOWLEDGMENTS

The authors acknowledge Science Foundation Ireland (Grant No. 08/SRC/B1412) for research funding under the Strategic Research Cluster program and (Grant Number 03/IN.3/1361/EC07) for FE-SEM imaging. We also thank Dr. Brendan Twamley, Mr. Maurice Burke and Prof. Peter Myer for their valuable technical support and assistance on FE-SEM, Raman spectroscopy and silica materials.

REFERENCES

(1) McCreery, R. L. *Chem. Rev.* **2008**, *108*, 2646−2687.
(2) Kim, S. N.; Rusling, J. F.; Papadimitrakopoulos, F. *Adv. Mater.* **2007**, *19*, 3214−3228.
(3) Song, J.; Xu, J.; Zhao, P.; Lu, L.; Bao, J. *Microchim. Acta* **2011**, *172*, 117−123.
(4) Ma, G.-X.; Lu, T.-H.; Xia, Y.-Y. *Bioelectrochemistry* **2007**, *71*, 180−185.
(5) Lu, X.; Zhou, J.; Lu, W.; Liu, Q.; Li, J. *Biosens. Bioelectron.* **2008**, *23*, 1236−1243.
(6) George, S.; Lee, H. K. *J. Phys. Chem. B* **2009**, *113*, 15445−15454.
(7) Liang, C.; Dai, S.; Guiochon, G. *Anal. Chem.* **2003**, *75*, 4904−4912.
(8) Bleda-Martínez, M. J.; Lozano-Castelló, D.; Morallón, E.; Cazorla-Amorós, D.; Linares-Solano, A. *Carbon* **2006**, *44*, 2642−2651.
(9) Stellwagen, E. *Nature* **1978**, *275*, 73−74.
(10) Faulkner, K. M.; Bonaventura, C.; Crumbliss, A. L. *J. Biol. Chem.* **1995**, *270*, 13604−13612.
(11) Heller, A. *Acc. Chem. Res.* **1990**, *23*, 128−134.
(12) Eltmimi, A. H.; Barron, L.; Rafferty, A.; Hanrahan, J. P.; Fedyanina, O.; Nesterenko, E.; Nesterenko, P. N.; Paull, B. *J. Sep. Sci.* **2010**, *33*, 1231−1243.
(13) (a) Guo, Z.; Chen, J.; Liu, H.; Cha, C. *Anal. Chim. Acta* **2008**, *607*, 30−36. (b) Hu, Y.; Sun, H.; Hu, N. *J. Colloid Interface Sci.* **2007**, *314*, 131−140.
(14) Liu, L.; Guo, L.-P.; Bo, X.-P.; Bai, J.; Cui, X.-J. *Anal. Chim. Acta* **2010**, *673*, 88−94.
(15) Xu, Y.; Hu, C.; Hu, S. *Anal. Chim. Acta* **2010**, *663*, 19−26.
(16) Oyama, N.; Anson, F. C. *J. Electroanal. Chem. Interfacial Electrochem.* **1986**, *199*, 467−470.
(17) Dresselhaus, M. S.; Jorio, A.; Hofmann, M.; Dresselhaus, G.; Saito, R. *Nano Lett.* **2010**, *10*, 751−758.
(18) Palecek, S. P.; Zydney, A. L. *J. Membr. Sci.* **1994**, *95*, 71−81.
(19) Causserand, C.; Kara, Y.; Aimar, P. *J. Membr. Sci.* **2001**, *186*, 165−181.
(20) Bajpai, A. K.; Sachdeva, R. *J. Appl. Polym. Sci.* **2002**, *85*, 1607−1618.
(21) Huang, Q.; Lu, Z.; Rusling, J. F. *Langmuir* **1996**, *12*, 5472−5480.
(22) Zhou, Y.; Hu, N.; Zeng, Y.; Rusling, J. F. *Langmuir* **2001**, *18*, 211−219.
(23) Wei, S.; Dandan, W.; Ruifang, G.; Kui, J. *Electrochem. Commun.* **2007**, *9*, 1159−1164.
(24) Laviron, E. *J. Electroanal. Chem. Interfacial Electrochem.* **1979**, *101*, 19−28.
(25) Zhao, Y.-D.; Bi, Y.-H.; Zhang, W.-D.; Luo, Q.-M. *Talanta* **2005**, *65*, 489−494.
(26) Yi, X.; Huang-Xian, J.; Hong-Yuan, C. *Anal. Biochem.* **2000**, *278*, 22−28.
(27) Wang, Y.; Chen, X.; Zhu, J.-J. *Electrochem. Commun.* **2009**, *11*, 323−326.
(28) Kamin, R. A.; Wilson, G. S. *Anal. Chem.* **1980**, *52*, 1198−1205.
(29) Norouzi, P.; Larijani, B.; Faridbod, F.; Ganjali, M. R. *Int. J. Electrochem. Sci.* **2010**, *5*, 1550−1562.
(30) Liu, P.; Zhang, X.; Feng, L.; Xiong, H.; Wang, S. *Am. J. Biomed. Sci.* **2011**, *3*, 69−76.
(31) Topoglidis, E.; Campbell, C. J.; Cass, A. E. G.; Durrant, J. R. *Electroanalysis* **2006**, *18*, 882−887.
(32) Xu, H.; Dai, H.; Chen, G. *Talanta* **2010**, *81*, 334−338.
(33) Liu, S.; Dai, Z.; Chen, H.; Ju, H. *Biosens. Bioelectron.* **2004**, *19*, 963−969.
(34) Yu, J.; Ju, H. *Anal. Chim. Acta* **2003**, *486*, 209−216.
(35) Song, J.; Xu, J.; Zhao, P.; Lu, L.; Bao, J. *Microchim. Acta* **2011**, *172*, 117−123.
(36) Gao, Y.-C.; Xi, K.; Wang, W.-N.; Jia, X.-D.; Zhu, J.-J. *Anal. Methods* **2011**, *3*, 2387−2391.